Laser fluence and spot size effect on compositional and structural properties of $BiFeO_3$ thin films grown by Pulsed Laser Deposition

N. Jaber[1], J. Wolfman[1†], C. Daumont[1], B. Négulescu[1], A. Ruyter[1], T. Sauvage[2], B. Courtois[2], H. Bouyanfif[3], J.L. Longuet[4], C. Autret-Lambert[1], F.Gervais[1]

1 Laboratoire GREMAN, UMR7347 CNRS Université François Rabelais, faculté de sciences et techniques 37200 Tours, France

2 Laboratoire CEMHTI, UPR3079 CNRS, Site Cyclotron 45071 Orléans cedex 2, France

3 Laboratoire LPMC, Université Jules Vernes Picardie - Amiens, France

4 CEA, DAM, Le Ripault, F-37260 Monts, France

[†]corresponding author: wolfman@univ-tours.fr

ABSTRACT

We investigated the effect of laser fluence and spot size on the structure and composition of $BiFeO_3$ (BFO) epitaxial thin films grown on $SrTiO_3$ substrates by pulsed laser deposition. X-ray diffraction shows that BFO's out of plane lattice parameter increases with the laser fluence. A coherent epitaxial film growth is observed for all tested laser fluences and spot sizes for thicknesses up to 16 nm. The critical thickness at which relaxation occurs depends either on the laser fluence or spot size. The fluence dependence of the out of plane lattice parameter is accompanied with a cationic composition variation. Bi vacancies are evidenced at lower fluences while as Bi/Fe tends towards 1 a higher relaxation critical thickness is observed. An optimum Bi/Fe ratio is obtained for a fluence of 1.72 J/cm^2. This result was confirmed by wavelength-dispersive x-ray spectroscopy (WDS) scans over a 1cm^2 film. An excellent thickness and composition uniformity is attained over the entire sample area.

KEYWORDS

Pulsed laser deposition; Excimer laser; Oxide thin film; $BiFeO_3$; WDS film analysis;

1. Introduction

Perovskites (ABO_3) and metal oxides with a structure deriving from it have been widely studied because of the large variety of physics phenomena, e.g. piezoelectricity, superconductivity, ferromagnetism, they exhibit. Their abundance and natural resistance to corrosion make them suitable materials for a wide range of applications. It is well known that perovskite physical properties are extremely sensitive to composition variation and defects which strongly influences their structure (e.g. oxygen-cation-oxygen bond angle, orbital ordering…) and symmetry [1]. A tight control of the stoichiometry is thus required, which is even more challenging in thin film form. One of the most studied materials in the last decade for its unique room-temperature multiferroic properties and their potential related applications is the rhombohedrically distorted perovskite $BiFeO_3$ (BFO) [2]. Indeed BFO is ferroelectric (T_c ~1100K [3] [4]) with record polarization (100 $\mu C.cm^{-2}$) and antiferromagnetic (T_N ~ 643K) [2]. Growing single phased $BiFeO_3$ thin films proved however to be a challenging task: Bi is highly volatile and parasitic phases such as Bi_2O_3 and Fe_2O_3 are easily formed. Non-stoichiometry and/or parasitic phases affect the magnetic [5], ferroelectric [6] and transport properties [7] of BFO in an undesired way. Pulsed Laser Deposition (PLD) is a very popular technique to grow multi-cationic epitaxial oxide films and has been widely used for BFO films [5] [8] [9] [10]. An intriguing fact is that although most authors report a narrow range of deposition conditions (oxygen partial pressure, substrate temperature, target stoichiometry…) leading to single phased BFO, these deposition

conditions vary widely from one research group to the other, as do the reported physical properties for the obtained films (maximum polarization, leakage current…). Such a spread in the published results suggests some off-stoichiometry in the synthetized films. One advantage of PLD compared to other Physical Vapor Deposition techniques is that the generated plasma during laser ablation contains all the cations present in the target with the same relative amount, independently of the cations masses. This however does not guarantee a stoichiometric transfer from the target to the film as many interactions occur in the expanding plasma (the "plume"): intra-plume collisions, electrostatic interactions (ions and electrons), diffusion by the ambient gas [11]. Depending on their mass and kinetic energy, species will have different radial distributions, more or less directional, influencing the local nucleation, growth, composition and thickness of the films [12]. At the origin of the plasma formation and transfer, laser fluence (or energy density), spot size and wavelength play a decisive role [13] [14] [15]. Several studies have investigated the effect of laser fluence / spot size on the A-site / B-site ratio in perovskite thin films of $SrTiO_3$ [16] [17] [18], $BaTiO_3$ [19] and $La_{0.7}Sr_{0.3}MnO_3$ [20] [21]. It has for example been shown that reducing the size of the laser spot (increasing fluence) creates an excess of A-site cations in $La_{0.7}Sr_{0.3}MnO_3$ films [20] [21] while the opposite trend is observed for $BaTiO_3$ [19]. To our knowledge such a study is lacking for BFO films and would give a new perspective on the large spread of published results. In this paper we investigated the laser fluence and spot size dependence of cationic stoichiometry and structure of $BiFeO_3$ thin films grown on $SrTiO_3$ substrates by PLD. In a second part we demonstrate a scanning scheme of the plume leading to a good uniformity of film thickness and stoichiometry over an area of $1cm^2$.

2. Experimental details

In this work, a KrF excimer laser with a wavelength of 248 nm, 25 ns pulses and a maximum pulse energy of 800 mJ was used (GSI Lumonics PM888). In order to study the effect of the laser fluence on BFO films, it is mandatory to start with a uniform energy distribution ("top hat" profile) of the laser impact on the target. The laser beam goes through an attenuator (Optec) to modulate the energy. A beam homogenizer with two crossed lenslet arrays (Coherent) is used to obtain a uniformly distributed energy in a plane where a mask with various square apertures is placed. An image of this mask is then projected and swept on the target surface (10 mm x 10 mm scanning area) via a projection lens and a deflecting mirror with motor-controlled positions in order to ensure focalization. A rotating sacrificial window (PVD product) is placed in front of the entrance window (vacuum side) to protect it from the deposit and maintain its transparency. The fluence is monitored inside the chamber a few centimeters above the target.

Growth conditions leading to a monophasic $BiFeO_3$ on $SrTiO_3$ (STO) substrate in our PLD system have been reported previously [22]. We used a Bi super-stoichiometric target ($Bi_{1.1}FeO_3$), a substrate temperature of 700°C, an oxygen pressure of 0.2 mbar, a pulse rate of 6 Hz with a target-substrate distance of 4.5 cm. Three different laser fluences were selected (1.65 J/cm^2, 1.32 J/cm^2 and 1 J/cm^2) playing with the attenuator while two laser impact area on the target surface were tested (1.51 mm^2 and 4.31 mm^2) thanks to two different square openings in the projected mask. A list detailing the various BFO deposited films is given in Table 1. Rutherford backscattering spectroscopy (RBS) was used to characterize the composition of the films and permitted to identify the optimal deposition fluence for stoichiometric BFO. Finally, the correct stoichiometry was confirmed by Wavelength-Dispersive X-ray Spectroscopy

(WDS) on an Electron Probe Micro-Analyzer equipped with four WDS spectrometers (WDS-EPMA SX50, Cameca).

3. Results and discussion

The X-ray diffraction patterns (Θ–2Θ scans) for the first set of films deposited with the smallest laser impact area (samples **I.a**, **I.b** and **I.c**) are presented in *figure 1a*), showing only (00l) peaks from BFO and STO and no sign of parasitic phases. The *figure 1b*) shows a zoom of these diagrams around the (001) peaks. A shift of the BFO (001) peak position to lower 2θ values is observed (cf. *figure 1b*) as the fluence increases, indicating an increase of the out of plane pseudo-cubic lattice parameter c_{pc} with laser fluence. As the deposition rate per pulse increases with laser fluence, the three samples of the first set are expected to have different thicknesses. This is indeed the case as can be seen from the reduction of the (001) peaks FWHM and from the period of the Laue oscillations as the fluence increases. Simulations of the diffraction patterns, fitting these two features, allowed us to estimate the thicknesses as indicated in *figure 1b*) and *c*) and table 1. Note that BFO epitaxial growth on STO leads to a compressive stress (BFO pseudo-cubic lattice parameter a_{pc} = 3.964Å versus a_{STO} = 3.905 Å) and relaxation beyond a critical thickness is expected. However, such a relaxation would lead to a decreased out of plane lattice parameter, while in our case we observe an increase with the thickness. So the evolution of lattice parameters described here cannot originate solely from different relaxation states and is most probably related to a composition variation (oxygen and/or cations content) with the fluence. X-ray diffraction patterns for the second set of samples deposited with the larger laser impact surface (sample **II.a**, **II.b** and **II.c$_1$**) are presented in *figure 1c*). A similar trend in the BFO (002) peak position versus laser fluence is observed for the two sets. This is clearly seen in

figure 1d) where the extrapolated c_{pc} lattice parameters are plotted versus fluence for the two sets. Note that the c_{pc} of film **II.a** compares more to that of film **I.a** (same fluence of 1.62 J/cm^2, twice thicker) than to that of film **I.b** (comparable thickness and different fluences). This confirms that the thickness, hence relaxation, is not the driving parameter for the observed c_{pc} variation.

To confirm epitaxial growth of the films and characterize a possible in plane relaxation, we measured reciprocal space maps (RSM) in the (*Qx, Qz*) plane around the $(103)_{STO}$ asymmetric reflection. In *figure 2* are reported the RSM for five of these films. The first four maps (2a-d) correspond to films deposited with the large impact surface. For the three tested fluences and thicknesses below 30 nm (fig 2a, 2b and 2c), reflections from the substrate and the film are vertically aligned, indicating a coherent epitaxial film growth (same in plane lattice parameter as STO). For a 49 nm thick BFO deposited at 1 J/cm^2 however (sample **II.c$_2$**), the film reflection is deformed and left-skewed indicating that some relaxation has occurred (fig. 2d). Interestingly, an even thicker film (62 nm, sample **I.a**) deposited at 1.62 J/cm^2 with the small laser impact surface (*figure 2e*) exhibit a slightly distorted reflection on its upper left part but still vertically aligned with substrate's reflection, probably corresponding to the onset of relaxation. The 49 nm thick film (sample **II.c$_2$** fig 2d) shows an advanced relaxed state compared to that of the 62 nm thick film (sample **Ia** fig. 2e). This implies that the relaxation threshold depends on either the laser fluence or the laser impact surface. Note that the peak vertical position of film **Ia** (fig. 2e) is the smallest of all five maps indicating that this strained film has the largest c_{pc} parameter of all.

To study the effect of laser fluence on the composition in our $BiFeO_3$ films, RBS ~~(Rutherford Backscattering Spectrometry)~~ measurements were carried out on the first set of films. An example of such a RBS spectrum is represented in *figure 3* for sample

I.a. During the measurement, the beam (2×2 mm^2) energy was 2000 keV with a resolution of 11 keV. The spectra are then simulated with SIMNRA software and Sr and Ti signals are taken as standards. The volume density of $BiFeO_3$ is estimated at 8.34 g/cm^3 with the pseudo-cubic lattice of the bulk material (a_{pc} ~ 3.964Å).

Film thicknesses extracted from the simulations (e.g. 60 ± 1 nm here in *figure 3*) are in close agreement with that estimated by XRD (62 nm ± 1 for **I.a**) as can be seen in *table 1*. However we note that although the simulation faithfully reproduces the peaks and plateaus associated with cations beyond the channel 400, it overstates the counts for channels below 350 keV where the small step from the oxygen atoms plateau arises. This problem, related to an under-estimation of the low keV penetrating particle energy straggling in SIMNRA software, prevent from a direct estimation of the oxygen content via the simulation. An indirect estimation of the oxygen content can in theory be made considering that the charge from oxygen signal balances the difference between the total measured charge and the charge from Bi and Fe signals. However the insulating nature of the substrate induces some errors in the measurement of the total charge and systemically led us to an overestimation of the oxygen content (see *table 2*). Comparison of direct and indirect measurements of the oxygen content, respectively by Nuclear Reaction Analysis (NRA not shown) and RBS, on another BFO film confirmed both the correct oxygen stoichiometry of our sample (59.5 ± 1.2 at.% by NRA for 60 at.% expected) and the RBS overestimation of the same content (61.2 ± 0.7 at. %) due to imperfect total charge estimation. Absolute atomic concentrations of Bi and Fe calculated from the over-estimated oxygen content are indicated in *table* 2; however the only relevant values are the Bi/Fe ratios which are discussed thereafter. Sample **I.a** is the one with the Bi/Fe ratio closest to 1 (0.99 ± 0.03). As the fluence decreases, the Bi/Fe ratio also decreases. This trend is clearly seen in *figure 4*. A dashed line, serving

as guide to the eye, intersects a Bi/Fe ratio equal to 1 for an optimal laser fluence of about 1.72 J/cm^2 for the small laser impact surface. The observed variation in the c_{pc} lattice parameter with laser fluence shown in *figure 1b)* for the first set of films can now be ascribed to a composition variation of these films.

As the c_{pc} lattice parameter varies in the same way in both sets of films (*figure 1d*), we assumed that the composition of BFO films was much more sensitive to the fluence than to the laser impact surface. To verify this hypothesis, we grew a $BiFeO_3$ film (sample III) using the large impact surface (A = 4.31 mm^2) with the estimated optimal laser fluence from the small laser impact set. The local stoichiometry and its spatial variation were measured by WDX to confirm the correct composition and assess thickness and composition homogeneity over 1 cm^2. A specific thin film analysis program has been used to determine BFO's composition (TFA/WDS layerf, Cameca). Analysis was performed with various incident electron beam energy (from 8 to 20 keV). Elements from the substrate were also measured. STO's density x thickness product ($\rho.t$) and composition were fixed in the TFA program. BFO film's density x thickness product and composition were simultaneously computed by the TFA program to fit the experimental k-ratio measurement for each element. From weight percentages determined by TFA/WDS analysis, atomic percentages can be determined and converted into Bi and Fe content x and y assuming the $Bi_xFe_yO_z$ formula with z = 3 and charge neutrality. Thirty measurements were realized with a beam diameter of 20 µm (20 keV and 100 nA) every 300 nm along the film. *Figure 5* represents the density × thickness ($\rho.t$) product and the weight percentages of Bi, Fe and O after self-consistent analysis of the raw data. The sum of the weight percentages is not imposed and amounts here to 99.5%, i.e. very close to the expected 100%, confirming the validity of the analysis. The average value of $\rho.t$ is 242 µg/cm^2 with a standard deviation of 5.4

µg/cm^2 equivalent to a relative variation of 2.2%. Considering the bulk BFO density (d = 8.38 g/cm^3) we find a thickness t = 289 nm ± 6.5 nm (1σ). This reflects the excellent thickness uniformity of our deposition process based on laser beam sweeping across a 10×10 mm^2 square on the target surface remaining in focus. Thickness uniformity is associated to compositional uniformity as there is an even greater stability of Bi and Fe weight percentages along the film. The average weight percentages and standard deviations are 66.51 ± 0.16 for the Bi and 17.73 ± 0.11 for Fe. The corresponding atomic percentages are respectively 20.02% ± 0.08% and 19.98% ± 0.08% for an expected value of 20%. With these statistical measurements we can conclude that we obtained the sought Bi/Fe ratio of 1 with a laser fluence of 1.72 J/cm^2 and large laser impact surface.

4. Conclusion

This work reports on the effect of laser fluence and spot size on structural and chemical properties of $BiFeO_3$ films. The BFO out of plane lattice parameter increases with the laser fluence in a similar way for the two tested laser spot sizes. RBS analysis on the films deposited with the small laser spot showed that the Bi/Fe ratio increases with the laser fluence and approaches 1 for a fluence of 1.72 J/cm^2. The local composition of a film deposited with the large laser spot size at 1.72 J/cm^2 was mapped by WDX along an 8 mm line. The Bi/Fe ratio of 1.000 ± 0.008 (1σ) was found along the sample, confirming that the parameter driving the Bi vacancies is the laser fluence and not the laser spot size. Furthermore we found that the lower the Bi vacancies the higher the critical relaxation thickness. Finally we underline the excellent composition and thickness uniformities achieved here, properties seldom reported for Pulsed Laser Deposited film in the literature.

ACKNOWLEDGMENTS

This work was supported by Region Centre (Oxymore project grant number 2011-64339).

REFERENCES

[1] M. Imada, A. Fujimori and Y. Tokura, “Metal-insulator transitions”, Rev. Mod. Phys., 70 1998) 1039.

[2] G. Catalan and J. F. Scott, “Physics and Applications of Bismuth Ferrite”, Adv. Mater., 21 (2009) 2463.

[3] W. Kaczmarek and Z. Pajak, “ Differential thermal analysis of phase transitions in $(Bi_{1-x}La_x)FeO_3$ solid solution”, Solid State Commun., 17 (1975) 807.

[4] Y. E. Roginskaya, Y. Y. Tomoshpolskii, Y. N. Venevstev, V. M. Petrov and G. S. Zhdanov, “The Nature of the Dielectric and Magnetic Properties of $BiFeO_3$”, Sov. Phys. - JETP, 23 (1966) 47.

[5] H. Béa, M. Bibes, A. Barthélémy, K. Bouzehouane, E. Jacquet, A. Khodan, J.-P. Contour, S. Fusil, F. Wyczisk, A. Forget, D. Lebeugle, D. Colson and M. Viret, “Influence of parasitic phases on the properties of BiFeO3 epitaxial thin films”, Appl. Phys. Lett. 87 (2005) 072508.

[6] T. Rojac, M. Kosec, B. Budic, N. Setter and D. Damjanovic, “Strong ferroelectric domain-wall pinning in BiFeO3 ceramics”, J. Appl. Phys., 108 (2010) 074107.

[7] Y. Nakamura, S. Nakashima and M. Okuyama, “Influences of Surface Texture and Bi/Fe Ratio on Electric Properties of $BiFeO_3$ Thin Films Prepared by Chemical Solution Deposition”, Jap. J. Appl. Phys., 47 (2008) 7250.

[8] K. Y. Yun, D. Ricinschi, T. Kanashima, M. Noda and M. Okuyama, “Giant Ferroelectric Polarization Beyond 150 μC/cm^2 in $BiFeO_3$ Thin Film”, Jap. J. Appl. Phys., 43 (2004) L647.

[9] W. Eerenstein, F. D. Morrison, J. Dho, M. G. Blamire, J. F. Scott and N. D. Mathur, “Comment on ‘‘Epitaxial $BiFeO_3$ Multiferroic Thin Film Heterostructures"” Sciences, 307 (2005) 1203a.

[10] V. R. Palkar, J. John and R. Pinto, “Observation of saturated polarization and dielectric anomaly in magnetoelectric $BiFeO_3$ thin films”, Appl. Phys. Lett., 80 (2002) 1628.

[11] K. Saenger, Pulsed Laser Deposition of Thin Films, ed. D.B. Chrisey and G.K. Hubler, John Wiley & Sons, New York:, 1994.

[12] T. Ohnishi, H. Koinuma and M. Lippmaa, “Pulsed laser deposition of oxide thin films”, Appl. Surf. Sci., 252 (2006) 2466.

[13] K. R. Chen, J. N. Leboeuf, R. F. Wood, D. B. Geohegan, J. M. Donato, C. L. Liu and A. A. Puretzky, “Mechanisms affecting kinetic energies of laser-ablated materials”, J. Vac. Sci. & Tech. a 14 (1996) 1111.

[14] D. B. Geohegan and A. A. Puretzky, “Dynamics of laser ablation plume penetration through low pressure background gases”, Appl. Phys. Lett., 67 (1995)197.

[15] R. F. Wood, K. R. Chen, J. N. Leboeuf, A. A. Puretzky and D. B. Geohegan, “Dynamics of Plume Propagation and Splitting during Pulsed-Laser Ablation”, Phys. Rev. Lett., 79 (1997) 1571.

[16] B. Dam, J. H. Rector, J. Johansson and J. Huijbregtse, “Mechanism of incongruent ablation of $SrTiO_3$”, J. Appl. Phys., 83 (1998) 3386.

[17] T. Ohnishi, M. Lippmaa, T. Yamamoto, S. Meguro and H. Koinuma, “Improved stoichiometry and misfit control in perovskite thin film formation at a critical fluence by pulsed laser deposition” Appl. Phys. Lett., 87 (2005) 241919.

[18] D. J. Keeble, S. Wicklein, R. Dittmann, L. Ravelli, R. A. Mackie and W. Egger, “Identification of A- and B-Site Cation Vacancy Defects in Perovskite Oxide Thin Films”, Phys. Rev. Lett., 105 (2010) 226102.

[19] D. Kan and Y. Shimakawa, “Controlled cation stoichiometry in pulsed laser deposition-grown $BaTiO_3$ epitaxial thin films with laser fluence”, Appl. Phys. Lett., 99 (2011) 081907.

[20] J. H. Song, T. Susaki and H. Y. Hwang, “Enhanced Thermodynamic Stability of Epitaxial Oxide Thin Films”, Adv. Mater., 20 (2008) 2528.

[21] L. Fitting Kourkoutis, J. H. Song, H. Y. Hwang and D. Muller, “Microscopic origins for stabilizing room-temperature ferromagnetism in ultrathin manganite layers,” PNAS, 107 (2010) 11682.

[22] N. Jaber, J. Wolfman, C. Daumont, B. Negulescu, A. Ruyter, G. Feuillard, M. Bavencoffe, J. Fortineau, T. Sauvage, B. Courtois, H. Bouyanfif, J. L. Longuet and F. Gervais, “Enhancement of piezoelectric response in Ga doped $BiFeO_3$ epitaxial thin films,” J. Appl. Phys., 117 (2015) 244107.

List of figure and table captions

Table 1: List of samples and deposition parameters. Thicknesses are estimated from XRD scans or WDX (III).

Table 2: Thicknesses, Bi, Fe and O atomic concentrations (at %) and Bi/Fe ratios for samples I.a, I.b and I.c extracted from RBS spectra simulations

Figure 1: (a) θ-2θ diffractograms of samples I.a, I.b and I.c. (b) Zoom around the (001) reflection of fig. 1a). (c) θ-2θ diffractograms around the (001) reflection of samples II.a, II.b and II.c. (d) Pseudo cubic out of plane lattice parameter as a function of laser fluence for the two laser impact surfaces.

Figure 2: Reciprocal space maps around the $(103)_{STO}$ reflections of samples (a) II.a, (b) II.b, (c) II.c1, (d) II.c2 and (e) I.a

Figure 3: RBS spectrum of the sample I.a

Figure 4: Evolution of Bi/Fe at. ratio, estimated from RBS measurements, with the laser fluence.

Figure 5: Evolutions of density × thickness product (ρ.t) and weight percentages of Bi, Fe and O as a function of the position for sample III.

Tables

Table 1

Samples	**I.a**	**I.b**	**I.c**	**II.a**	**II.b**	**II.c_1**	**II.c_2**	**III**
Laser Fluence F (J/cm^2)	1.62	1.32	1	1.62	1.32	1		1.72
Laser impact surface A (mm^2)	1.51			4.31				4.31
Number of Pulses	40000	60000	60000	4500	10000	21000	65000	26600
Thickness (nm)	62	35	17	30	21	16	49	289

Table 2

	Thickness	**Bi**	**Fe**	**O**	**Bi/Fe**
Theoretical value (at %)		20	20	60	**1**
Sample I.a (1.62 J/cm^2) (at %)	60 ± 1 nm	18.7 ± 0.2	18.8 ± 0.5	62.5 ± 0.7	**0.99 ± 0.03**
Sample I.b (1.32 J/cm^2) (at %)	35 ± 1 nm	18.7 ± 0.3	19.5 ± 0.5	61.8 ± 0.8	**0.96 ± 0.03**
Sample I.c (1.00 J/cm^2) (at %)	17 ± 1 nm	17.2 ± 0.3	18.9 ± 0.5	63.9 ± 0.8	**0.91 ± 0.03**

Tables 1

Samples	**I.a**	**I.b**	**I.c**	**II.a**	**II.b**	**II.c$_1$**	**II.c$_2$**	**III**
Laser Fluence F (J/cm^2)	1.62	1.32	1	1.62	1.32	1		1.72
Laser impact surface A (mm^2)	1.51			4.31				4.31
Number of Pulses	40000	60000	60000	4500	10000	21000	65000	26600
Thickness (nm)	62	35	17	30	21	16	49	289

Tables 2

	Thickness	Bi	Fe	O	Bi/Fe
Theoretical value (at %)		20	20	60	**1**
Sample I.a (1.62 J/cm^2) (at %)	60 ± 1 nm	18.7 ± 0.2	18.8 ± 0.5	62.5 ± 0.7	**0.99 ± 0.03**
Sample I.b (1.32 J/cm^2) (at %)	35 ± 1 nm	18.7 ± 0.3	19.5 ± 0.5	61.8 ± 0.8	**0.96 ± 0.03**
Sample I.c (1.00 J/cm^2) (at %)	17 ± 1 nm	17.2 ± 0.3	18.9 ± 0.5	63.9 ± 0.8	**0.91 ± 0.03**

Figures 1

Click here to download Figures (if any): Figure 1_rev.pdf

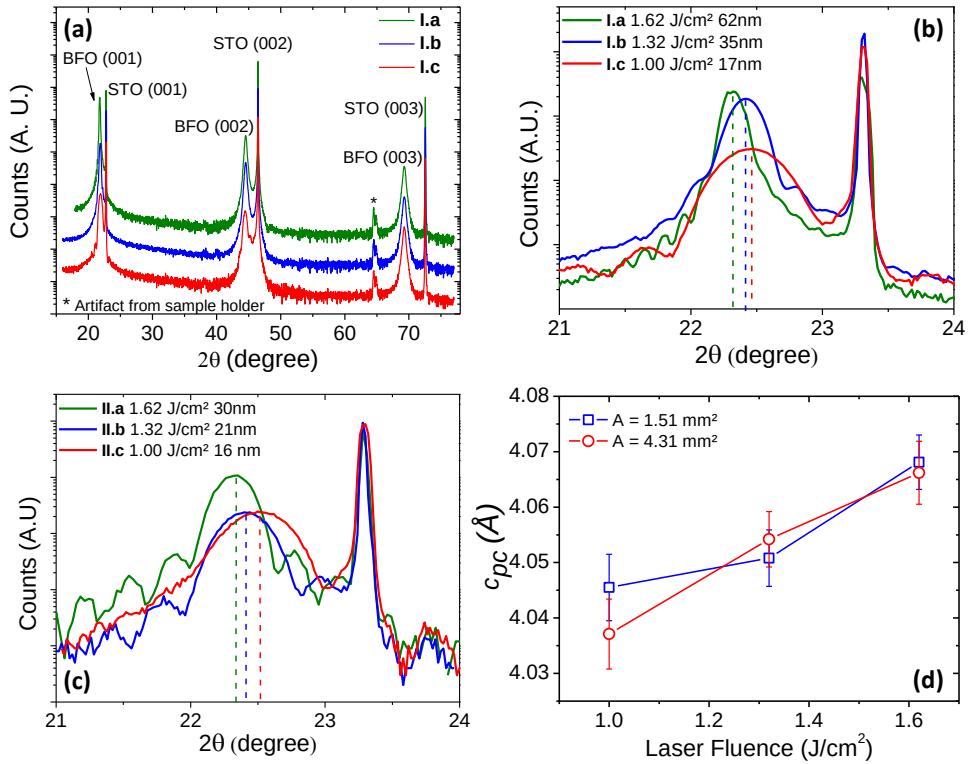

Figures 2

Click here to download Figures (if any): Figure 2_rev.pdf

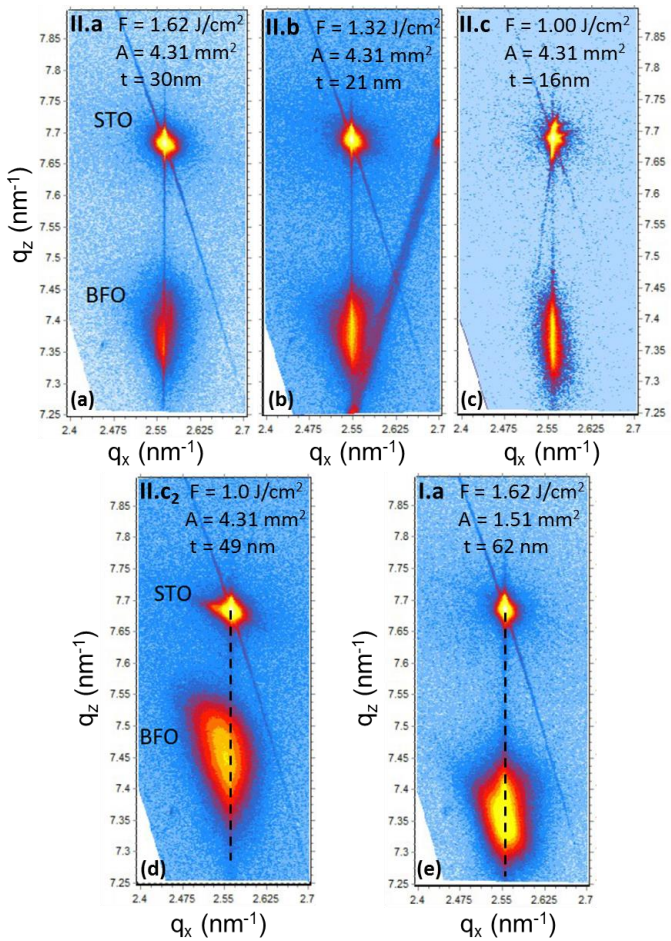

Figures 3

Click here to download Figures (if any): Figure 3.pdf

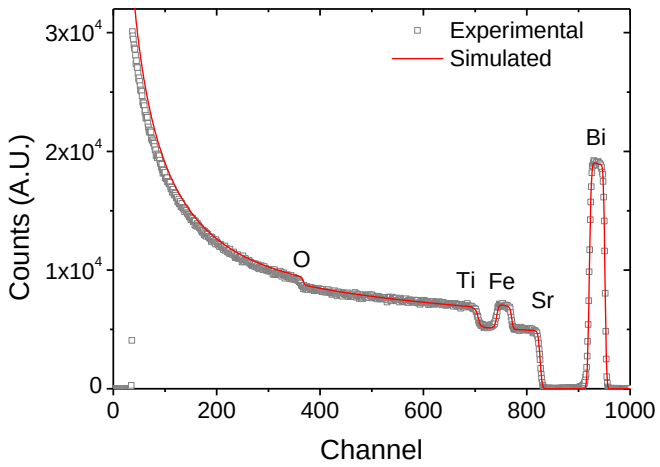

Figures 4

Click here to download Figures (if any): Figure 4 v2.pdf

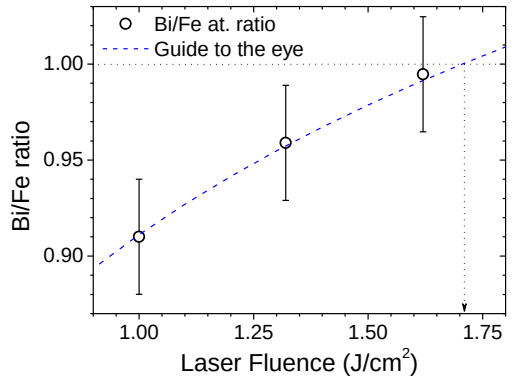

Figures 5

Click here to download Figures (if any): Figure 5.pdf